

Structure of Native and Expanded Sobemoviruses by Electron Cryo-Microscopy and Image Reconstruction

Natacha Opalka^{1,2}, Mariana Tihova², Christophe Brugidou³
Abhinav Kumar⁴, Roger N. Beachy¹, Claude M. Fauquet³
and Mark Yeager^{2,4,5*}

¹Division of Plant Biology

²Department of Cell Biology

³International Laboratory for Tropical Agricultural Biotechnology (ILTAB/ORSTOM-TSRI), Division of Plant Biology

⁴Department of Molecular Biology, The Scripps Research Institute, 10550 North Torrey Pines Road, La Jolla CA 92037, USA

⁵Scripps Clinic, Division of Cardiovascular Diseases, 10666 North Torrey Pines Road, La Jolla, CA 92037, USA

Rice yellow mottle virus (RYMV) and southern bean mosaic virus, cowpea strain (SCPMV) are members of the Sobemovirus genus of RNA-containing viruses. We used electron cryo-microscopy (cryo-EM) and icosahedral image analysis to examine the native structures of these two viruses at 25 Å resolution. Both viruses have a single tightly packed capsid layer with 180 subunits assembled on a $T = 3$ icosahedral lattice. Distinctive crown-like pentamers emanate from the 12 5-fold axes of symmetry. The exterior face of SCPMV displays deep valleys along the 2-fold axes and protrusions at the quasi-3-fold axes. While having a similar topography, the surface of RYMV is comparatively smooth. Two concentric shells of density reside beneath the capsid layer of RYMV and SCPMV, which we interpret as ordered regions of genomic RNA. In the presence of divalent cations, SCPMV particles swell and fracture, whereas the expanded form of RYMV is stable. We previously proposed that the cell-to-cell movement of RYMV in xylem involves chelation of Ca^{2+} from pit membranes of infected cells, thereby stabilizing the capsid shells and allowing a pathway for spread of RYMV through destabilized membranes. In the context of this model, we propose that the expanded form of RYMV is an intermediate in the *in vivo* assembly of virions.

© 2000 Academic Press

Keywords: virus structure; electron cryo-microscopy; image processing; sobemovirus

*Corresponding author

Introduction

Rice yellow mottle virus (RYMV) and southern bean mosaic virus (SBMV) are members of the genus Sobemovirus. First reported in Kenya (Bakker, 1974), the disease caused by RYMV is now widespread in many western and eastern African countries. SBMV exclusively infects Leguminosae and has been reported from the United States, Central and South America, Africa, France and India. The cowpea strain (SCPMV) used in this study infects most cowpea cultivars (Shepherd & Fulton, 1962) and induces mosaic and leaf distortions. The genomes of RYMV and SCPMV consist of a single molecule of positive sense RNA with a 5'-linked protein (VPg). The complete genome sequences of RYMV (Ngon A Yassi *et al.*, 1994) and SCPMV (Wu *et al.*, 1987) reveal four open reading frames designated ORFs 1 to 4, predicted to encode at least four proteins. ORF1 of RYMV encodes a protein of 17.8 kDa that is involved in virus movement (Bonneau *et al.*, 1998). The functions of the

Present addresses: N. Opalka, Laboratory of Molecular Biophysics, The Rockefeller University, 1230 York Avenue, New York, NY 10021, USA; C. Brugidou, Institut de recherche Pour le développement, 911 Avenue Agropolis, BP5045, 34032 Montpellier cedex 1, France; A. Kumar, University of Washington, Health Sciences Center, K-428, Box 357742, Seattle, WA 98195, USA; R. N. Beachy, Donald Danforth Plant Science Center, 7425 Forsyth Boulevard, Suite 385, Box 1098, St. Louis, MO 63105, USA; C. M. Fauquet, ILTAB/Donald Danforth Plant Science Center, 8001 Natural Bridge Road, St. Louis, MO 63121, USA.

Abbreviations used: BPMV, bean pod mottle virus; CCMV, cowpea chlorotic mottle comovirus; LTSV, lucerne transient streak virus; RYMV, rice yellow mottle virus; SsbMV, sesbania mosaic virus; SBMV, southern bean mosaic virus - bean; SCPMV, southern bean mosaic virus - cowpea; TBSV, tomato bushy stunt virus; TYMV, turnip yellow mosaic tymovirus; cryo-EM, electron microscopy.

E-mail address of the corresponding author: yeager@scripps.edu

ORF1 and ORF3 proteins remain unknown. By comparison with other RNA viruses, ORF2 encodes a polyprotein that apparently includes the VPg, a protease and a polymerase. ORF4 encodes the coat protein of 26 kDa for RYMV and 28 kDa for SCPMV.

The pairwise similarity between the sequences for the capsid proteins of SCPMV and RYMV is only 20.1% (Table 1). In contrast, the sequences of SBMV, SCPMV and sesbania mosaic virus (SsbMV) display much greater similarity (Table 1). Despite the presence of a number of substitutions in the N-terminal region of RYMV compared to SCPMV, the residues in this region are highly basic, a property thought to be important for protein-RNA interactions and for the stability of the virion. Ngon a Yassi *et al.* (1994) also proposed that the N-terminal region of the coat protein of RYMV and SCPMV has a bipartite nuclear targeting motif, which could account for the presence of virions in the nuclei of infected cells (Francki *et al.*, 1985). The stability of the capsid shell of sobemoviruses is known to be dependent on the chelation of Mg^{2+} and Ca^{2+} (Hsu *et al.*, 1976). Although RYMV displays little sequence similarity with SCPMV, all amino acids involved in Ca^{2+} binding in SCPMV (D157, D160, E213, N278) are conserved in RYMV, except for E213 (Figure 1).

The X-ray structure of the cowpea strain of couther bean mosaic virus (SCPMV) at 2.8 Å resolution displays a solid capsid shell composed of 180 identical protein subunits, which assemble with $T = 3$ icosahedral symmetry (Abad-Zapatero *et al.*, 1980). The protein subunit consists of two domains. The R (random) domain (residues 1 to 64, 7 kDa) is partially ordered, and the S (shell) domain (residues 65 to 260, 21 kDa) displays a canonical β -barrel motif. The highly basic N-terminal region of the coat protein is thought to interact with RNA to stabilize the virion. For example, removal of amino-terminal residues (1 to 30) results in the assembly of particles with a $T = 1$ capsid shell (Savithri & Erickson, 1983).

Interactions that are important for the *in vitro* stability of the sobemoviruses include a divalent cation protein-protein bond, a pH-dependent protein-protein link and protein-RNA interactions (Hull, 1977). Upon alkali treatment in the presence

of divalent cation chelators, the capsid shell swells and becomes sensitive to enzymes and denaturants. Such swelling has been demonstrated for other plant viruses and may represent an intermediate state before disassembly and release of the RNA for binding by ribosomes and subsequent translation (Wilson, 1985). Interestingly, poliovirus undergoes capsid swelling during receptor attachment (Fricks & Hogle, 1990). However, the expansion of cowpea chlorotic mottle comovirus (CCMV) was not required for disassembly and translation of viral RNA (Albert *et al.*, 1997).

Here, we report a comparison of the three-dimensional structures of RYMV and SCPMV at 25 Å resolution derived from electron micrographs of unstained, frozen-hydrated specimens. Although the capsid proteins exhibit only 20.1% similarity, the subunits assemble on a $T = 3$ icosahedral lattice, and the capsid surfaces display similar protrusions clustered around the 5-fold axes of symmetry. Although the swollen form of SCPMV was unstable, the swollen form of RYMV was more stable and amenable to image analysis. We propose that this expanded form of RYMV is an intermediate in the *in vivo* assembly of virions.

Results

Electron cryo-microscopy and image processing

Native frozen-hydrated particles of RYMV and SCPMV exhibited distinctive circular and hexagonal profiles when examined by electron cryo-microscopy (Figure 2(a) and (b)). The absence of distortion and the constant size of the particles confirmed good preservation of the vitrified sample. Although the particle edges were smooth, structural features were clearly visible within the particle boundaries. In the presence of EDTA, many of the SCPMV particles swelled and fractured (Figure 2(d), background), whereas the swollen RYMV particles were stable and had a size close to that of native SCPMV (Figure 2(c)).

Differences in the appearance of the individual particle images of RYMV and SCPMV were consistent with random orientations of the virions in the vitrified buffer, as was confirmed by a plot of

Table 1. Coat protein sequence comparisons in the *Sobemovirus* genus

	CfMV	LTSV	RYMV	SBMV	SCPMV	SsbMV
CfMV	-	18.9	30.5	18.5	19.3	19.3
LTSV	75.8	-	22.2	23.8	23.0	26.4
RYMV	66.9	75.2	-	20.5	20.1	18.4
SBMV	75.2	67.8	73.5	-	75.9	69.0
SCPMV	75.7	66.0	75.8	23.8	-	62.8
SsbMV	75.7	66.0	77.5	30.4	36.8	-

The upper right shows the percentage similarity between individual pairs, and the lower left shows the percentage divergence.

CfMV, cocksfoot mottle virus (Mäkinen *et al.*, 1995); LTSV, lucerne transient streak virus (Jeffries *et al.*, 1995); RYMV, rice yellow mottle virus (Ngon A Yassi *et al.*, 1994); SBMV, southern bean mosaic virus (Othman and Hull, 1995); SCPMV, southern cowpea mosaic virus (Wu *et al.*, 1987); SsbMV, sesbania mosaic virus (Bhuvaneshwari *et al.*, 1995).

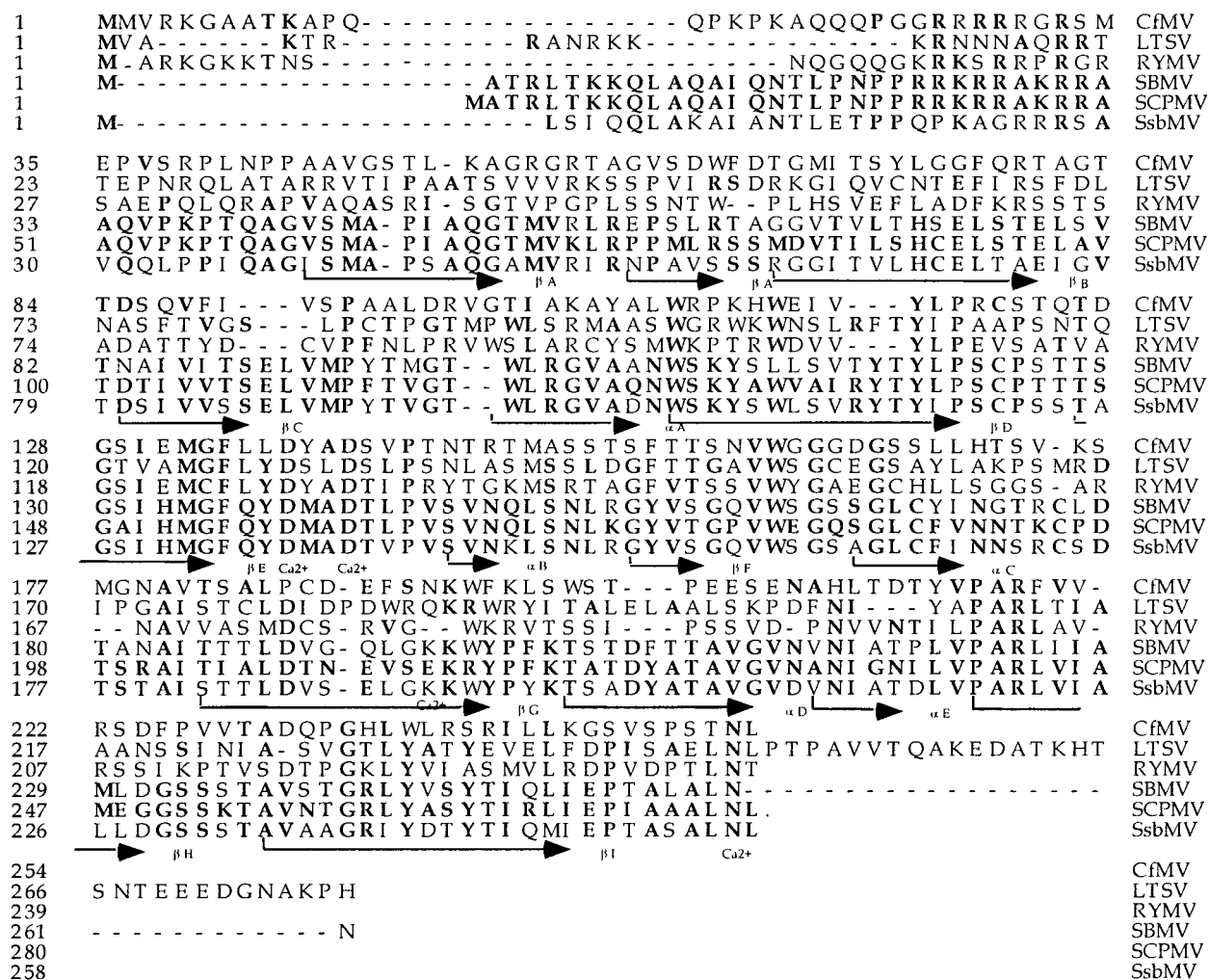


Figure 1. Alignment of the coat protein sequences of CfMV, LTSV, RYMV, SBMV, SCPMV and SsbMV. Bold letters identify identical residues. The locations for β -sheets, α -helices and Ca^{2+} -binding sites are based on their positions in the X-ray crystal structure of SCPMV.

the particle orientations over the icosahedral asymmetric unit (Figure 3(a)). Eigenvalue spectra provide a test for errors resulting from a non-random distribution of particle orientations (Crowther *et al.*, 1970). For both the compact forms of RYMV and SCPMV, and the expanded form of RYMV, the inverse eigenvalues were less than 0.1, which confirmed that the three-dimensional reconstructions were reliably determined. Based on a cross-correlation cut-off value of 0.5, the resolution was ~ 25 Å for the maps of native RYMV and SCPMV and ~ 35 Å for the map of swollen RYMV (Figure 3(b)). The inability to refine the map of swollen RYMV to higher resolution may reflect heterogeneity due to a decrease of stability upon expansion.

Three-dimensional reconstructions of native RYMV and SCPMV

As was evident in the images, the three-dimensional reconstructions of native RYMV and

SCPMV revealed a single, solid capsid shell that was hexagonal when viewed down the 2-fold and 3-fold axes of symmetry and circular when viewed down the 5-fold vertex positions (Figure 4). The capsid shells were composed of 12 pentamers and 20 hexamers arranged on a $T = 3$ icosahedral symmetry lattice. Both viruses displayed pentameric protrusions around the 5-fold axes of symmetry, which extended from radii of ~ 153 to ~ 160 Å for RYMV and from ~ 155 to ~ 164 Å for SCPMV (Figure 4). The protrusions at the 3-fold axes of symmetry were less prominent. Around the quasi-3-fold axes, SCPMV displayed a slightly higher mass of density than for RYMV. The distance between the trimers was also shorter in SCPMV than for RYMV (~ 53 Å for SCPMV and ~ 59 Å for RYMV).

Protein distribution in native RYMV and SCPMV

Plots of the spherically averaged density of the native, compact forms of RYMV and SCPMV

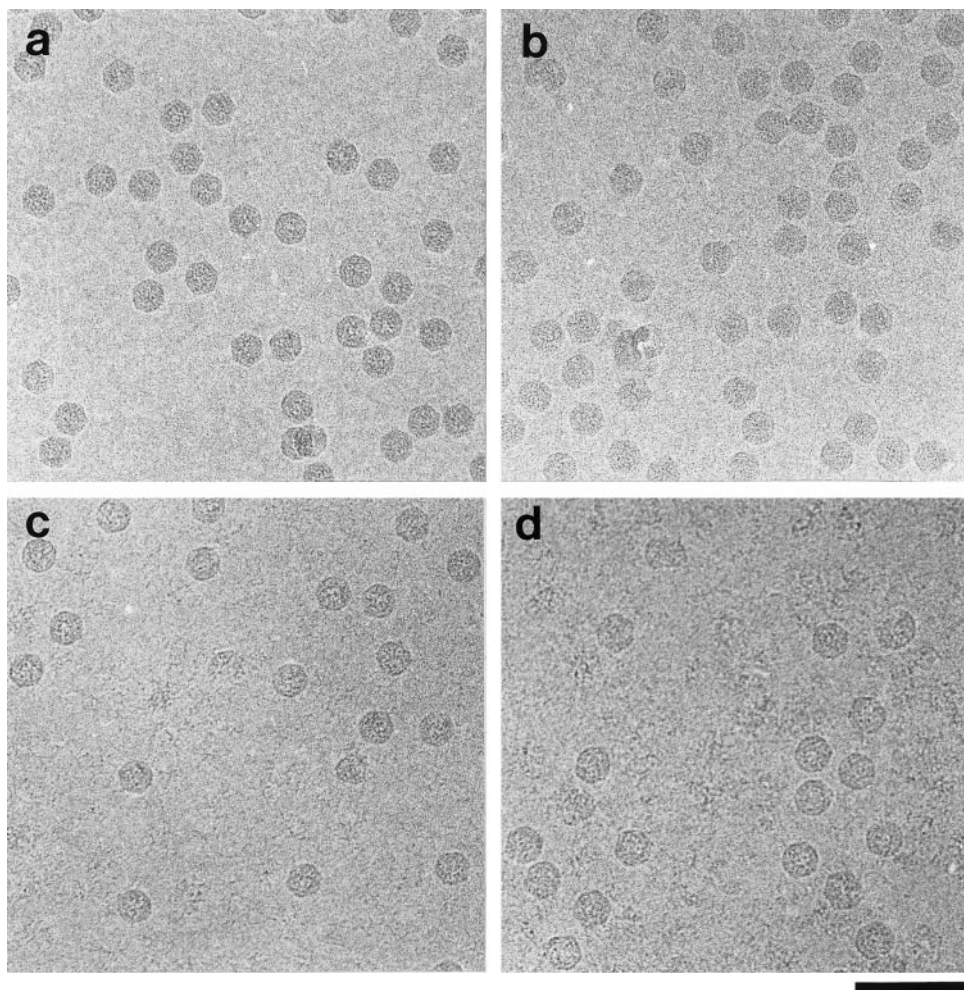


Figure 2. Electron micrographs of unstained, frozen-hydrated (a) native RYMV, (b) native SCPMV, (c) swollen RYMV and (d) swollen SCPMV. The native particles (a) and (b) are of uniform size and exhibit circular and hexagonal profiles. Samples of (c) swollen RYMV showed more uniformly sized particles compared with (d) swollen SCPMV in which the particles were more irregular and the background showed fragments of fractured particles. The scale bar represents 1000 Å

reconstructions revealed capsid shells centered at radii of 130 and 138 Å, respectively (Figure 5). The isosurface values for the protein shells displayed in Figures 4, 6, and 8 to 11 were adjusted to yield volumes for RYMV and SCPMV of 5.75×10^6 Å³ and 6.19×10^6 Å³, respectively, based on $T = 3$ capsid shells formed by 180 subunits of molecular mass 26 kDa (for RYMV) and 28 kDa (for SCPMV), assuming a protein partial specific volume of 0.74 cm³/g. Sectioned views of the RYMV and SCPMV three-dimensional reconstructions along the 2-fold symmetry axis revealed solid capsid shells with hexagonal profiles and protrusions at the 5-fold axes (Figure 6(a) and (b)). However, the curvature and thickness of the capsid shell varied. The RYMV capsid exhibited a fairly smooth surface relief. The thickness was nearly constant except at the inner surface of the 5-fold axes where cavities were observed. In contrast, the inner surface of the SCPMV capsid showed a larger mass of density at the 5-fold axes. In addition,

there were distinct protrusions along the quasi-3-fold axes that extended to a radius of 151 Å, and depressions were seen at the 2-fold axes in the exterior face.

Ordered shells of RNA in native RYMV and SCPMV

As expected, the radial density plot of the X-ray map of SCPMV revealed no density within the capsid shell (Figure 5). The slight rippling with small peaks at ~61 and ~89 Å are ascribed to Fourier series termination error because the ~28 Å distance between these peaks is close to the cut-off resolution of 25 Å. Note that the inner peaks labelled I and II in the RYMV and SCPMV profiles were substantially larger, which we interpret as organized regions of genomic RNA that adopt a partial icosahedral arrangement. Peaks I and II were centered at ~96 and ~56 Å for RYMV and ~101 and ~65 Å for SCPMV. The isosurface values

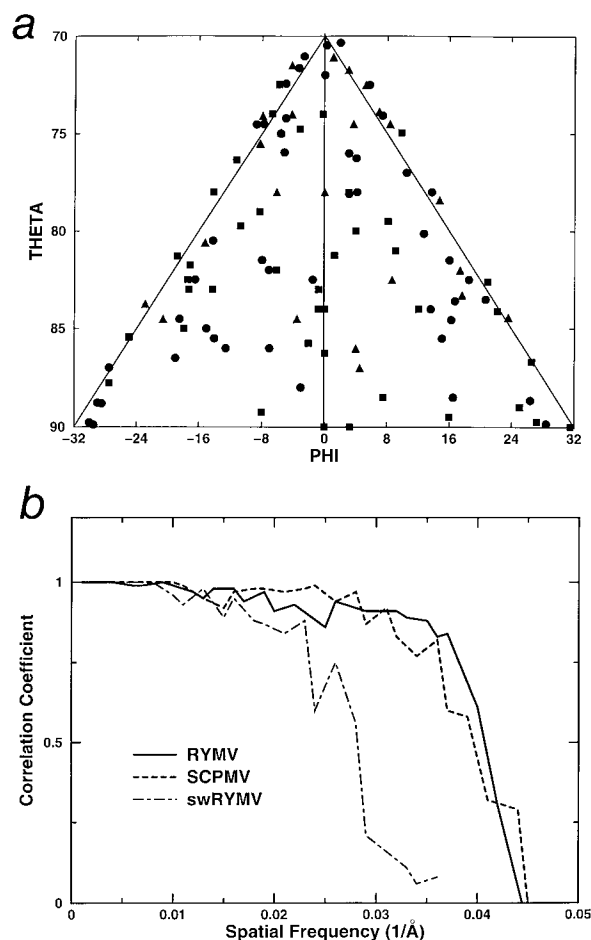


Figure 3. (a) Plot of the refined θ , ϕ orientation angles for native RYMV (●), SCPMV (■) and swollen RYMV (▲) particles. The plot demonstrates that the data encompass a fairly uniform distribution of orientations. (b) Cross-correlation analysis. The particle image data sets were divided in half, and two independent reconstructions were computed. The maps for native RYMV (—), SCPMV (-----) and swollen RYMV (-·-·-·-) were compared as a function of spatial frequency. The correlation coefficients fall to a value of 0.5 at a resolution of ~ 25 Å for the native RYMV and SCPMV reconstructions and ~ 35 Å for swollen RYMV.

for these shells displayed in Figures 6, 7 and 11 were adjusted to yield volumes for the RYMV and SBCMV RNA of 1.4×10^6 Å³, based on the size of the genomic RNA (4.4 kB), assuming an anhydrous RNA partial specific volume of 0.55 cm³/g. Surface-shaded maps (Figure 7) showed that the two layers have a hexagonal shape when viewed down a 2-fold axis of symmetry and were formed by an open fenestrated network of density. For RYMV, layer I had projections at the 5-fold axes that extended to a radius of ~ 120 Å (Figure 7). Connections were also observed between layer I and the capsid shell at the 2-fold axes. Layer II had a distinctive dodecahedral shape in which densities at the 5-fold vertices were connecting by rod-like

densities suggestive of duplex RNA. The two internal layers of density were less well defined in SCPMV. The outermost layer was more rounded, and there was no connection between the globular densities. Similarly, layer II displayed globular densities clustered at the 5-fold vertex positions.

Comparison of cryo-EM and X-ray maps of SCPMV

A density map derived from the 2.8 Å resolution X-ray structure of SCPMV was computed at 25 Å resolution and then rescaled by a factor of 3% to match the cryo-EM map. There was a remarkably close correspondence in the surface and internal contours of the X-ray and cryo-EM maps (Figure 8), which provided confidence that the SCPMV cryo-EM structure was reliably determined. This close similarity was confirmed by a correlation coefficient of 0.84 between these two reconstructions.

Comparison of SCPMV X-ray model and cryo-EM maps of native RYMV and SCPMV

A comparison between the X-ray model and the cryo-EM map of SCPMV was first performed without any rigid body refinement and yielded an *R*-factor of 0.56 (Figure 9(a)). After rigid body refinement, a best fit was obtained with a substantially improved *R*-factor of 0.36 (Figures 9(b) and 10(a)). A similar fit of the SCPMV X-ray model into the cryo-EM map of RYMV yielded an *R*-factor of 0.28 (Figures 9(c) and 10(b)).

Comparison of native and swollen RYMV

Upon chelation of divalent cations with EDTA, RYMV and SCPMV expand from peak radii of ~ 130 to ~ 139 Å and ~ 138 to ~ 148 Å, respectively (Figure 5). Specimens of swollen SCPMV contained numerous broken particles (Figure 2(d)), and for the most spherical particles, unique orientations could not be derived, which precluded determination of a three-dimensional reconstruction. Although specimens of RYMV contained far fewer broken particles, the three-dimensional reconstruction could be derived only to 35 Å resolution, compared with a resolution of 25 Å for the native particle. Therefore, the swollen particles are less stable and more heterogeneous in size.

The three-dimensional reconstruction of swollen RYMV exhibited similar features with the compact form (Figure 11(a)). Although the expanded particle was rounder, the hexagonal shape was maintained, and protrusions were seen at the 5-fold axis. The expansion was most notable at the icosahedral 2-fold and 5-fold axes where the diameter increased $\sim 8\%$. As noted, the two internal layers of density within RYMV are interpreted as ordered regions of genomic RNA (Figure 11(b) and (c) left), which were also seen in the expanded particle (Figure 11(b) and (c) right). Particle expansion generated a smoother inner

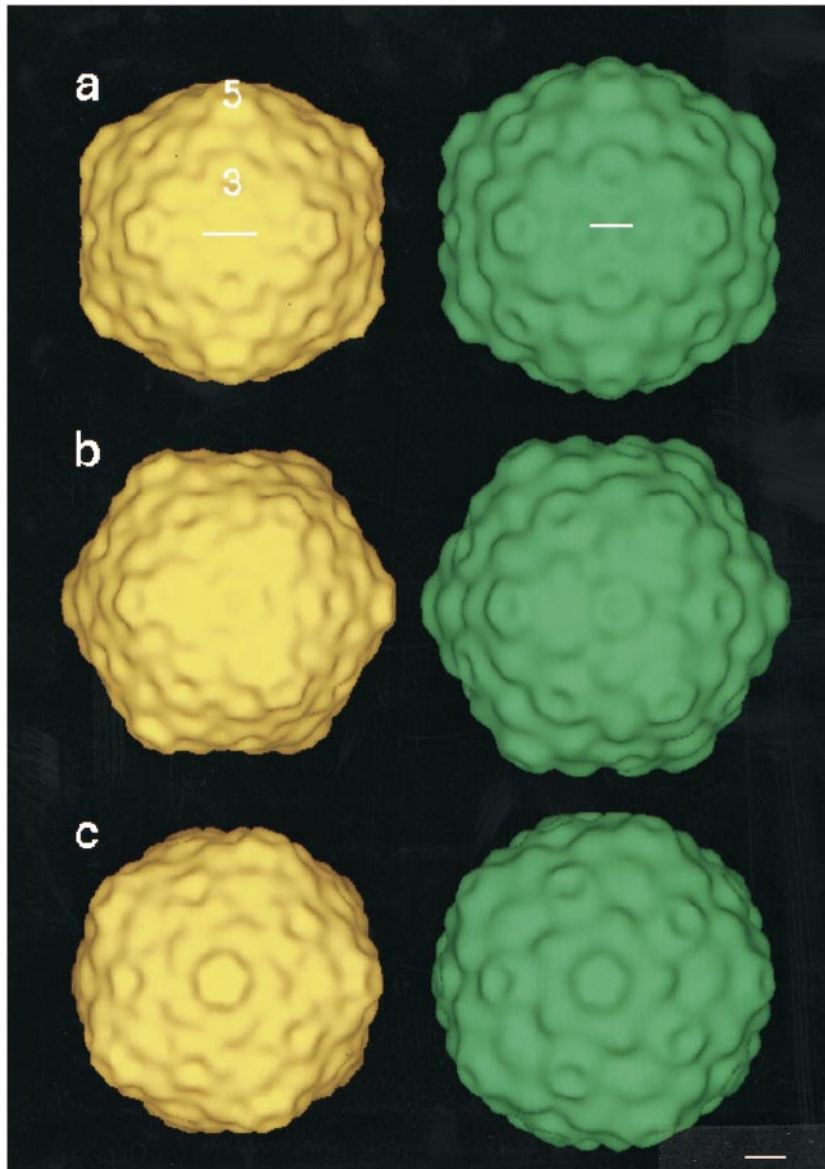


Figure 4. Three-dimensional, surface-shaded density maps of RYMV (left) and SCPMV (right), viewed down (a) 2-fold, (b) 3-fold and (c) 5-fold axes of symmetry. Both viruses display a solid capsid surface with protrusions at the 5-fold vertex positions. The 5-fold and 3-fold symmetry axes are indicated in (a). The ends of the bars in (a) identify the quasi-3-fold axes. The lengths of the bars indicate that the protrusions at the quasi-3-fold axes are separated by 59 Å in RYMV and 53 Å in SCPMV. The scale bar represents 40 Å.

surface (Figure 11(b) right) with loss of the cavity beneath the 5-fold symmetry axis seen in the native particle (Figure 11(b) left).

Discussion

Icosahedral capsid structure of RYMV and SCPMV and comparison with other $T=3$ plant viruses

Even though the sequence similarity between RYMV and SCPMV is only 20% (Figure 1) and the diameter of RYMV is $\sim 7\%$ smaller (Figure 5), there is conservation of $T=3$ icosahedral lattice

symmetry and considerable similarity in the topology of the capsid shells (Figure 4). We are impressed that three out of the four presumed Ca^{2+} -binding residues are conserved in RYMV (Figure 1). Lastly, the fit of the SCPMV atomic model to the RYMV density is surprisingly good (Figures 9(c) and 10(b)). Therefore, we expect that the canonical β -fold and subunit packing within SCPMV will be conserved in RYMV. Nevertheless, there are likely to be important differences in structure, since the swollen form of SCPMV is much more unstable than RYMV.

Both RYMV and SCPMV display prominent protrusions at the 5-fold vertex positions. Turnip yel-

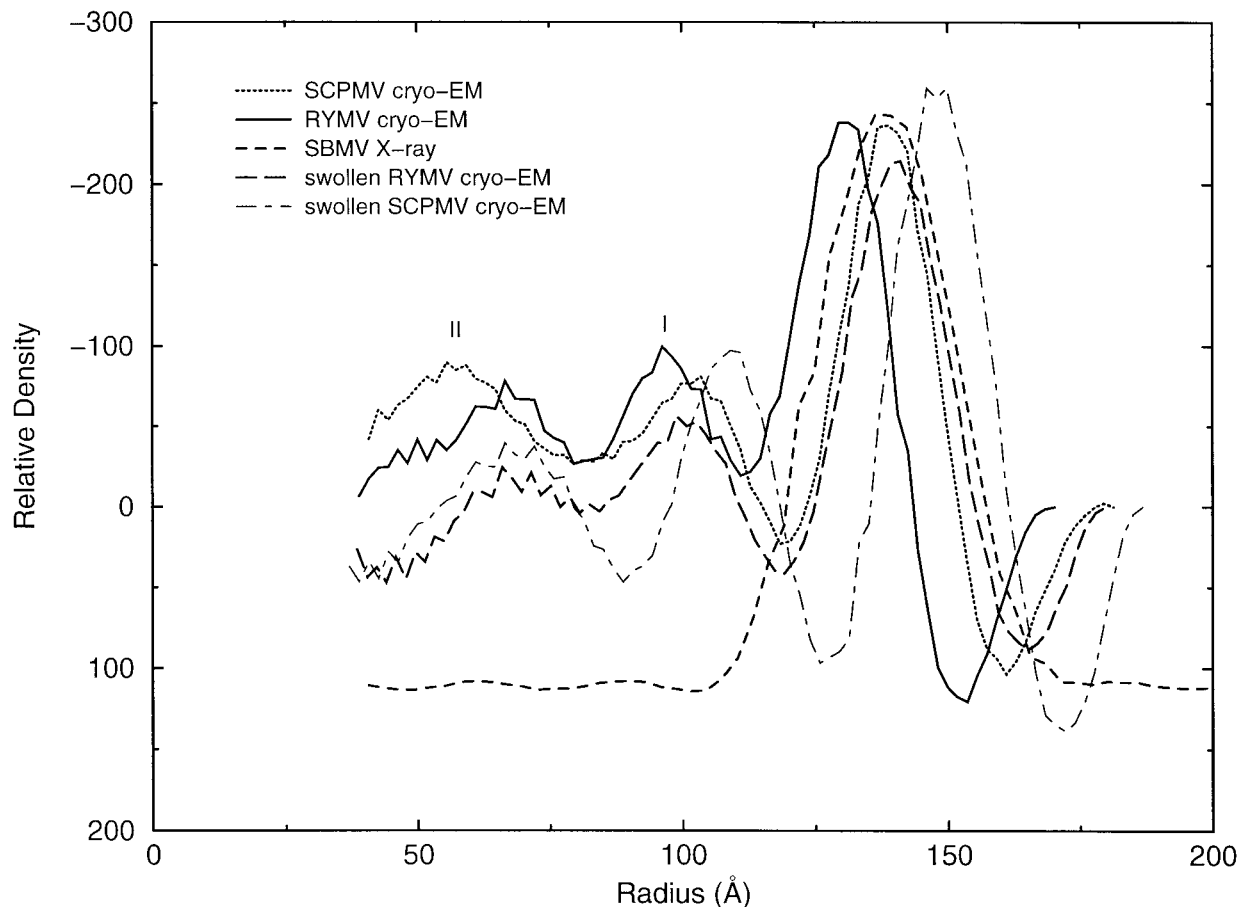


Figure 5. Radial density profiles of RYMV (—), SCPMV (·····), swollen RYMV (----), swollen SCPMV (-----) and SCPMV X-ray (-----) derived by spherically averaging the three-dimensional maps. The capsid shells are centered at peak radii of ~ 130 and ~ 138 Å for native RYMV and SCPMV. The shells expand to peak radii of ~ 139 and ~ 148 Å for swollen RYMV and SCPMV, respectively. The profiles derived from the cryo-EM maps show two inner peaks (labeled I and II) at radii of ~ 96 and ~ 65 Å for native RYMV, ~ 101 and ~ 56 Å for native SCPMV, and ~ 100 and ~ 66 Å for swollen RYMV. In comparison, the radial density profile derived from the X-ray map of SCPMV shows only slight rippling (small peaks at ~ 89 and ~ 61 Å), which we ascribe to Fourier series termination errors because the distance between these peaks (~ 28 Å) is close to the cut-off resolution of 25 Å. The substantial peaks I and II in the cryo-EM profiles are therefore ascribed to encapsidated RNA.

low mosaic virus (TYMV, genus Tymovirus) (Böttcher & Crowther, 1996; Canady *et al.*, 1996) and CCMV (Speir *et al.*, 1995) exhibit $T=3$ icosahedral symmetry with pentameric protrusions at the 5-fold axes. In addition, there are hexameric protrusions at the quasi-6-fold positions, which make these viruses appear less angular than RYMV and SCPMV. Association of the N termini of six subunits at the quasi-6-fold symmetry axis is a unique feature of TYMV and CCMV. Previous studies on $T=3$ plant viruses showed that the N termini of only three subunits interact at the quasi-6-fold symmetry axes (Olson *et al.*, 1983; Hogle *et al.*, 1986; Silva & Rossmann, 1987). In tomato bushy stunt virus, the protruding P domains reside at the quasi-3-fold axes (Olson *et al.*, 1983). The maps of SCPMV derived by X-ray crystallography and cryo-EM also reveal small protrusions at the quasi-3-fold axes, which arise from the

insertion of a three-turn helix (α D helix) and a one-turn helix (α E helix) (Abad-Zapareto *et al.*, 1980). These protrusions are less prominent in the cryo-EM structure of RYMV (Figures 4 and 10(b)). Interestingly, the RYMV sequence displays a deletion in the region corresponding to the α D helix as well as proline residues that would tend to break α -helices. (In Figure 1, compare the sequence ATDYA-TAVGVNAN in SCPMV with SI---PSSVD-PN for RYMV). These differences may account for the reduced height of the protrusions at the quasi-3-fold axes in the RYMV cryo-EM map.

Despite the similarity between pentamers and hexamers on the exterior surface of RYMV and SCPMV, the interior surfaces differ. For RYMV, there are cavities at the pentameric axes, which are also present in the capsid shell of TYMV (Canady *et al.*, 1996). In the case of CCMV, a channel is present in the pentamers which may be a consequence

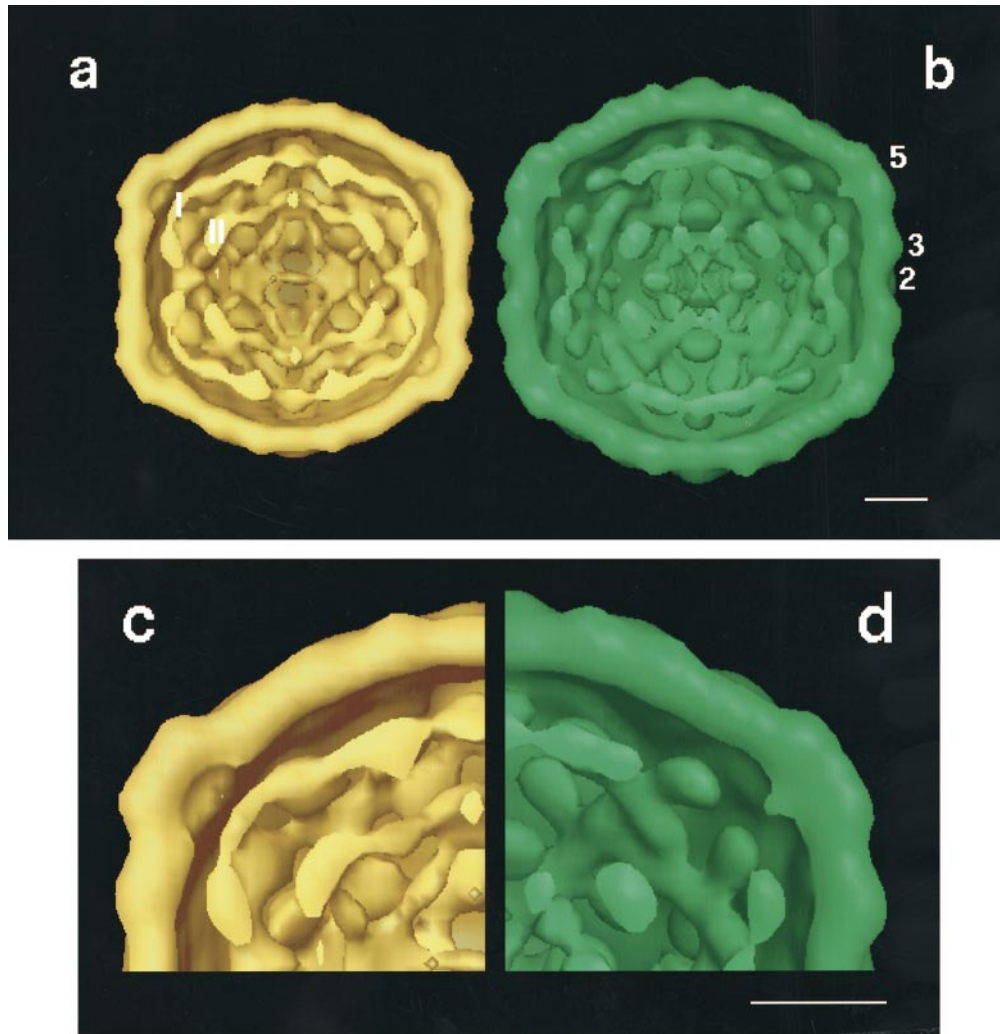


Figure 6. Surface-shaded sectioned views of (a) and (c) RYMV and (b) and (d) SCPMV show a solid capsid shell with two distinct concentric internal layers of density. These inner layers are ascribed to ordered regions of genomic RNA and give rise to peaks I and II in the radial density profiles (Figure 5). The close-up octant views of (c) RYMV and (d) SCPMV reveal an internal cavity beneath the 5-fold vertex position in RYMV that is not seen in SCPMV. The scale bar represents 40 Å.

of a different orientation of the subunits. Examination of the X-ray structure and the coat protein sequence of SCPMV suggests that the density beneath the 5-fold axis of symmetry arises from a polypeptide loop connecting β strand F and the α C helix and a loop connecting the α C helix and β strand G. Even though the SCPMV and RYMV coat proteins exhibit a high degree of homology within these loops (see Figure 1), this region of the RYMV coat protein may be splayed apart or disordered because a cavity is present beneath the 5-fold axis of symmetry (compare Figure 6(c) and (d) with Figure 9(a) and (c)). Alternatively, this cavity may, at least in part, be occupied by RNA in SCPMV, as is suggested by the additional density on the inner surface of the cryo-EM map of SCPMV at the 5-fold axes (Figure 8 bottom, left) compared with the X-ray map (Figure 8 bottom, right).

Ordered genomic RNA in sobemoviruses

X-ray crystallography has revealed partial icosahedral arrangement of the RNA within the capsid shell for three plant viruses with $T = 3$ symmetry, bean pod mottle virus (BPMV, genus Comovirus) (Chen *et al.*, 1989), cowpea chlorotic mottle virus (Speir *et al.*, 1995) and TYMV (Canady *et al.*, 1996). The icosahedral symmetry of the capsid shell may impose icosahedral ordering on some portions of the RNA. The cryo-EM maps of RYMV and SCPMV show two internal layers of density that we attribute to ordered genomic RNA. This interpretation is consistent with ordered regions of internal density seen in cryo-EM maps of *Nudaurelia capensis* β virus, a $T = 4$ insect virus (Olson *et al.*, 1990), rotavirus SA11 (Prasad *et al.*, 1996) and TYMV (Böttcher & Crowther, 1996) that has been ascribed to ordered regions of the genome. The

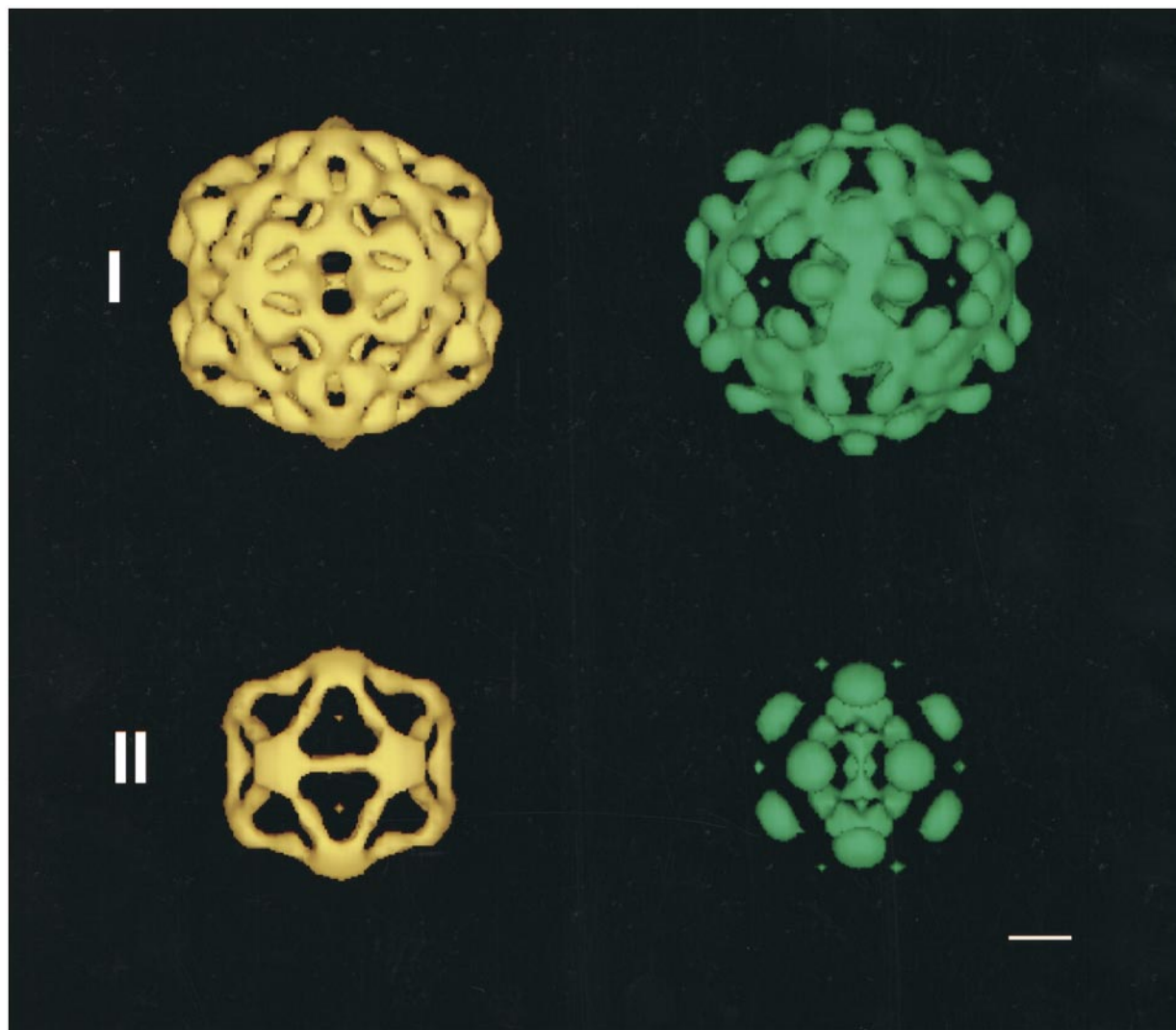


Figure 7. The inner shells of RYMV (left) and SCPMV (right) (labeled I and II, here, and in Figure 5) are ascribed to ordered regions of genomic RNA. The dodecahedral appearance of shell II for RYMV is consistent with ordered duplex RNA. The scale bar represents 40 Å.

RNA within the capsid shell of RYMV appears more ordered than that of SCPMV. For example, the dodecahedral appearance of layer II in RYMV (Figure 7) presumably corresponds to duplex RNA, which is not seen in SCPMV. These differences may be related to weaker protein-RNA interactions resulting from difference in the amino acid sequences or biochemical differences such as pH and/or ionic strength. (Note that the RYMV particles were maintained at pH 7, whereas the SCPMV particles were maintained at pH 5.5.)

Small-angle neutron scattering of SCPMV provided information on the distribution of the RNA and protein within the capsid shell (Krüse *et al.*, 1982). The scattering curves were consistent with a model having four concentric shells centered at radii of 40, 67, 97 and 126 Å. The outermost layer was assigned to the capsid shell, whereas the concentric shells at lower radii contained significant amounts of both RNA and some protein. The

results were consistent with localization of RNA and 15% of the protein within the interior of the capsid. The viral RNA was confined to radii less than 110 Å, in agreement with our results. The scattering profiles were interpreted by a model with a bilobal distribution of RNA and protein, similar to TBSV (Chauvin *et al.*, 1978).

Compact and expanded forms of plant viruses

Chelation of divalent cations by EDTA results in expansion of RYMV and SCPMV. Previous studies on the swollen forms of TBSV and CCMV showed that the expansion is triggered by electrostatic repulsion at the Ca^{2+} -binding sites located near the quasi-3-fold axes (Robinson & Harrison, 1982; Speir *et al.*, 1995). This repulsion caused a large conformational change with formation of holes at the quasi-3-fold axes. We presume that a similar mechanism may cause expansion in RYMV and

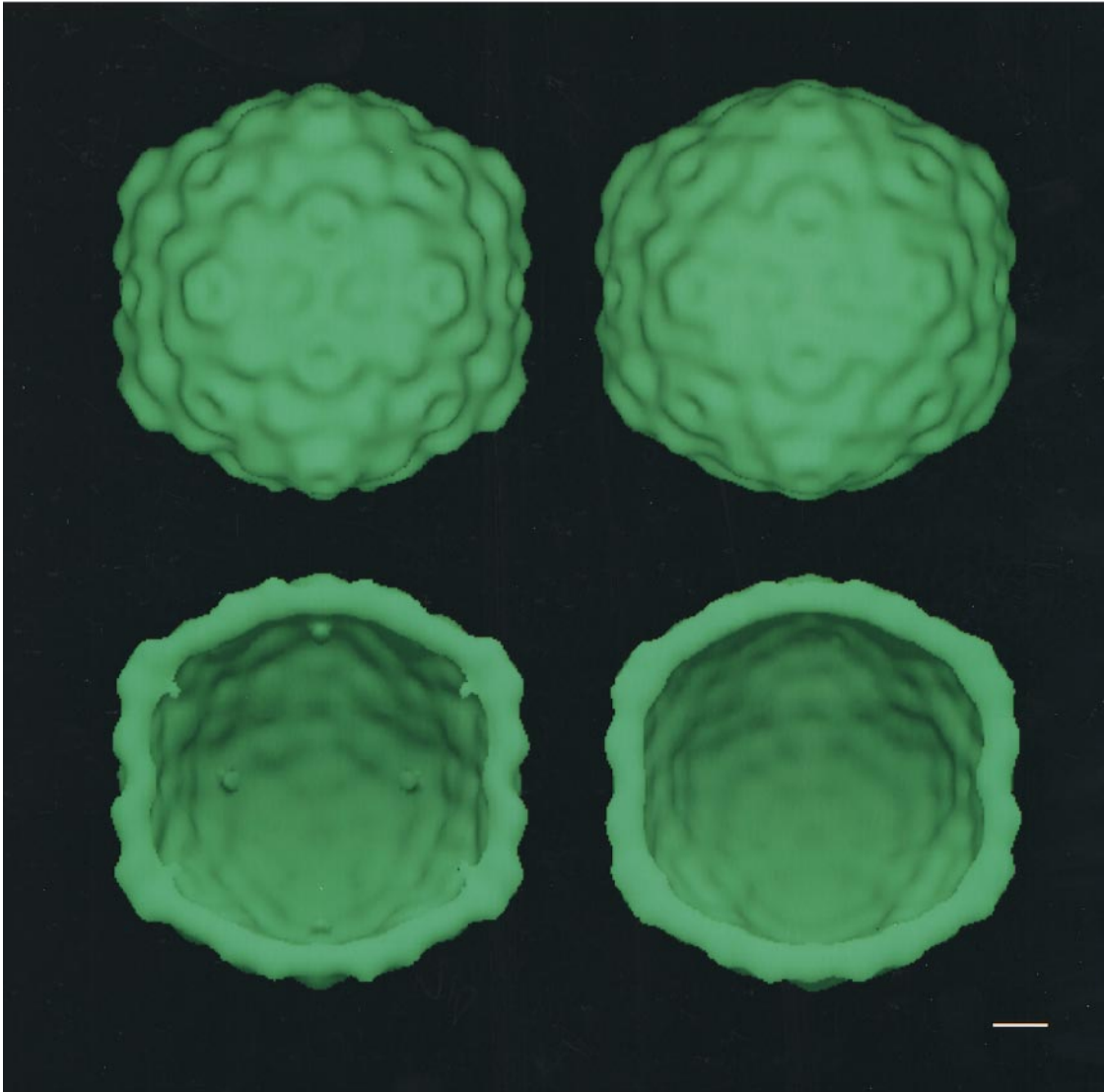


Figure 8. Three-dimensional surface-shaded density maps of SCPMV derived by cryo-EM (left) and X-ray crystallography (right) at 25 Å resolution. Note the close correspondence in the structure of the outer and inner surfaces of the capsid shell. To facilitate comparison with the X-ray structure, the two internal shells of density in the cryo-EM map (see Figure 7) were removed. The additional density on the inner surface of the cryo-EM map of SCPMV at the 5-fold axes (Figure 8 bottom, left) compared with the X-ray map (Figure 8 bottom, right) may be due to RNA in contact with the capsid at this site. The scale bar represents 40 Å.

SCPMV, since the X-ray structure of SCPMV does show bound Ca^{2+} , and three out of four of these residues are conserved in the RYMV amino acid sequence. The lack of holes at the quasi-3-fold axes in the expanded form of RYMV is presumably due to the low resolution of the reconstruction. Compared with RYMV, SCPMV particles tend to break during chelation of divalent cations, suggesting that SCPMV is more unstable upon swelling. This loss of stability could be due to weakening of protein-protein and/or protein-RNA associations. The N-terminal polypeptide of both capsid proteins may interact with the genome in a different manner after swelling. For instance, the expanded form of TBSV undergoes a rearrangement of the N ter-

mini of the A and B subunits, which become ordered and fold as β -sheets across the quasi-2-fold axes (Robinson & Harrison, 1982).

Functional implications

We previously examined the translocation pathway of RYMV in systemically infected leaves and the ultrastructural changes associated with RYMV infection using Western immunoblotting, Northern blotting and thin-section electron microscopy (Opalka *et al.*, 1998). In inoculated leaves, RYMV RNA and coat protein were first detected at three and five days post-inoculation, respectively. By six days post-inoculation, RYMV had spread systemi-

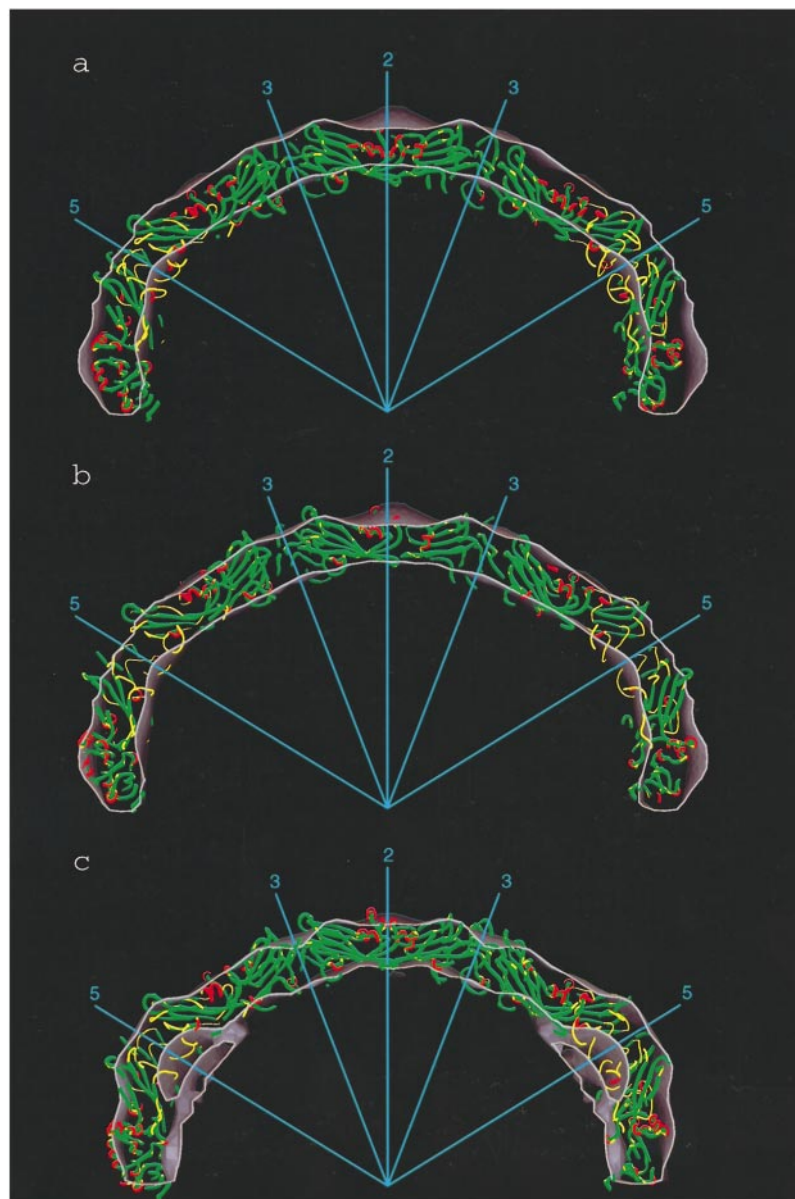


Figure 9. A ribbon diagram depicting the atomic structure of SCPMV has been docked within the molecular envelope provided by cryo-EM and image analysis, (a) before and (b) after rigid-body refinement. (b) After rigid-body refinement, there is close correspondence between the X-ray and cryo-EM maps. (c) The good correspondence between the atomic structure of SCPMV and the RYMV cryo-EM map suggests conservation in the protein fold, in spite of little sequence similarity between the SCPMV and RYMV coat proteins.

cally to leaves, and virus particles were observed in most cell types, including epidermal, mesophyll, bundle sheath, and vascular parenchymal cells. Most of the virions accumulated in large crystalline patches in xylem parenchyma cells and sieve elements. Colocalization of a cell wall marker for cellulosic β -(1-4)-D-glucans and RYMV antibodies over pit membranes suggested a pathway for virus migration between vessels. We proposed that the partial digestion of pit membranes resulting from programmed cell death may permit virus migration through them, concomitant with autolysis. In addition, displacement of Ca^{2+} from pit membranes to virus particles may contribute to the disruption of the pit membranes and facilitate systemic virus transport. In the context of this model, we propose that the expanded form of RYMV is an intermediate in the *in vivo* assembly of virions. Since the native particle map could be refined to

higher resolution compared with the swollen, we presume that the compact form is an inherently more stable particle with closer packing of subunits to protect the encapsidated genome.

Materials and Methods

Virus preparation

RYMV-CI from the Ivory Coast (referred to here as RYMV) was purified from infected rice plants (*Oryza sativa* L. variety IR8) as described (Fauquet & Thouvenel, 1977). RYMV was retrieved from a 10% to 40% (w/v) continuous sucrose gradient. Samples (1 to 3 ml) were then dialysed for 12 hours at 4°C against 500 ml of 20 mM potassium phosphate buffer (pH 7.0). SCPMV (kindly provided by Dr David Hacker) was isolated from cowpea plants according to the method of Johnson *et al.* (1974), in which the virus is purified by sequential precipitation in 8% (w/v) polyethylene glycol. The final

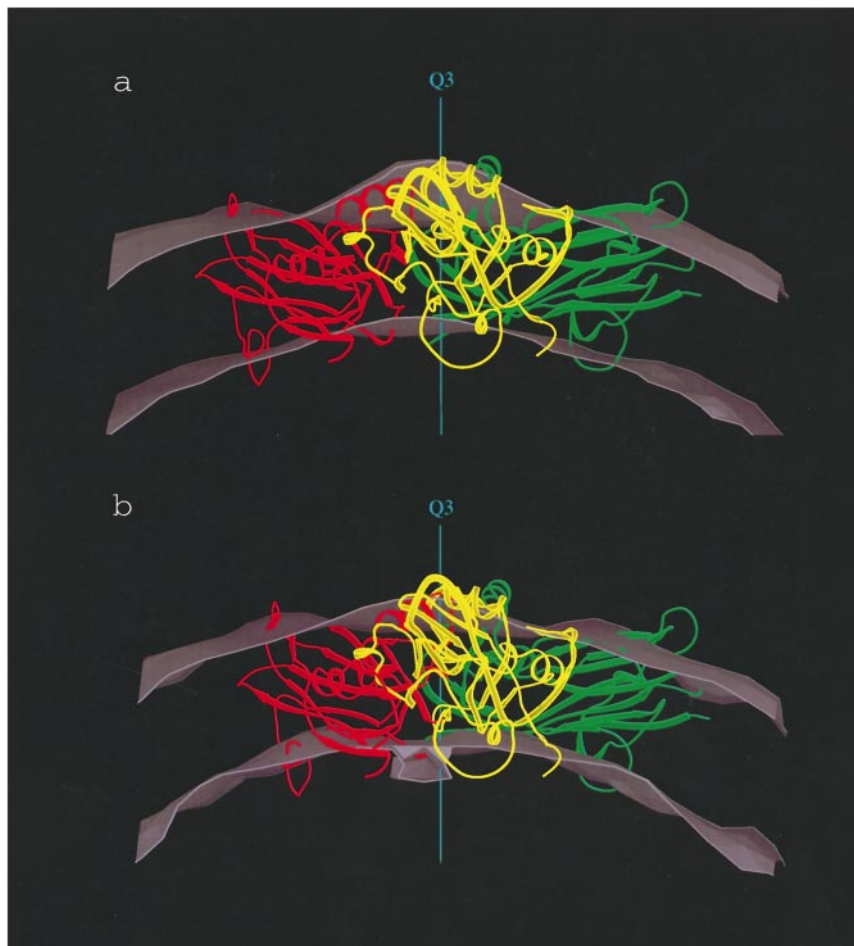


Figure 10. Ribbon diagrams depicting the atomic structures of the A (yellow), B (red) and C (green) subunits of SCPMV docked within the (a) SCPMV and (b) RYMV cryo-EM map. Protrusions at the quasi-3-fold axis are more prominent in the cryo-EM map of SCPMV than in the RYMV map. The polypeptide containing the α D and α E helices in the X-ray structure of SCPMV closely matches the SCPMV cryo-EM map at the quasi-3-fold axis. Notably, the corresponding region in the RYMV sequence contains a deletion as well as a proline residue. These sequence differences may account for the reduced height of the protrusions at the quasi-3-fold axes in the RYMV cryo-EM map (located at the tips of the bars in Figure 4(a)).

pellet after ultracentrifugation was resuspended at 3 to 5 mg/ml in 10 mM sodium acetate (pH 5.2).

Preparation of expanded particles

Swollen particles were prepared by a modification of the procedure of Rayment *et al.* (1979). Purified samples of native virions were dialysed for 24 hours at 4°C against 50 mM potassium phosphate buffer (pH 7.5) containing EDTA. Different concentrations of EDTA (10 mM, 20 mM and 30 mM) were used in order to define the appropriate conditions for cryo-EM. After ultracentrifugation for two hours, the pellet was resuspended in 20 mM potassium phosphate buffer (pH 7.5) containing 10 mM EDTA.

Electron cryo-microscopy

Aliquots of the virus suspension were applied to electron microscope grids coated with holey carbon film previously made hydrophilic by glow-discharge in an atmosphere of amylamine (Yeager *et al.*, 1994). Virus particles tended to preferentially adhere to the carbon rather than partition into the holes filled with vitrified buffer. This problem was solved by sequential application of two 5 μ l droplets of sample (\sim 5 mg/ml) to the grids. The first application of the sample to the grid presumably saturated non-specific binding sites of the virus to the carbon. The grid was blotted with filter paper, and a second 5 μ l aliquot was applied. After 60 seconds, the

droplet was blotted for eight seconds with preheated filter-paper and then immediately plunged into a slush of liquid ethane (Yeager *et al.*, 1990).

Grids were transferred to a Gatan 626 cryo-specimen holder (Gatan, Inc., Warrendale, PA) under liquid nitrogen and rapidly inserted into a Philips CM120 transmission electron microscope operated at 100 kV. Grids were examined at low magnification (3600 \times) to identify holes with minimal contamination and uniform ice thickness. The area just adjacent to the region to be photographed was examined at high magnification (88,000 \times) to locate Gaussian focus, correct for astigmatism and ensure that drift was minimal. Low dose (5 to 10 electrons/ \AA^2) micrographs were recorded at 0.8 to 1.2 μ m underfocus and a magnification of 45,000 \times .

Image processing

Optical diffraction was used to select images that displayed minimal astigmatism and drift based on the Thon rings in the contrast transfer function. Selected images were digitized at a 25 μ m interval using a Perkin Elmer microdensitometer, corresponding to 5.5 \AA on the specimen. A DEC Alpha equipped with a Denali graphics accelerator was used for image processing. The program X3D, kindly provided by Drs James Conway and Alasdair Steven, was used to extract particle images with a circular mask and subtract a background density. For processing the images of native RYMV, an initial set of origin and orientation values of 126 particles from a

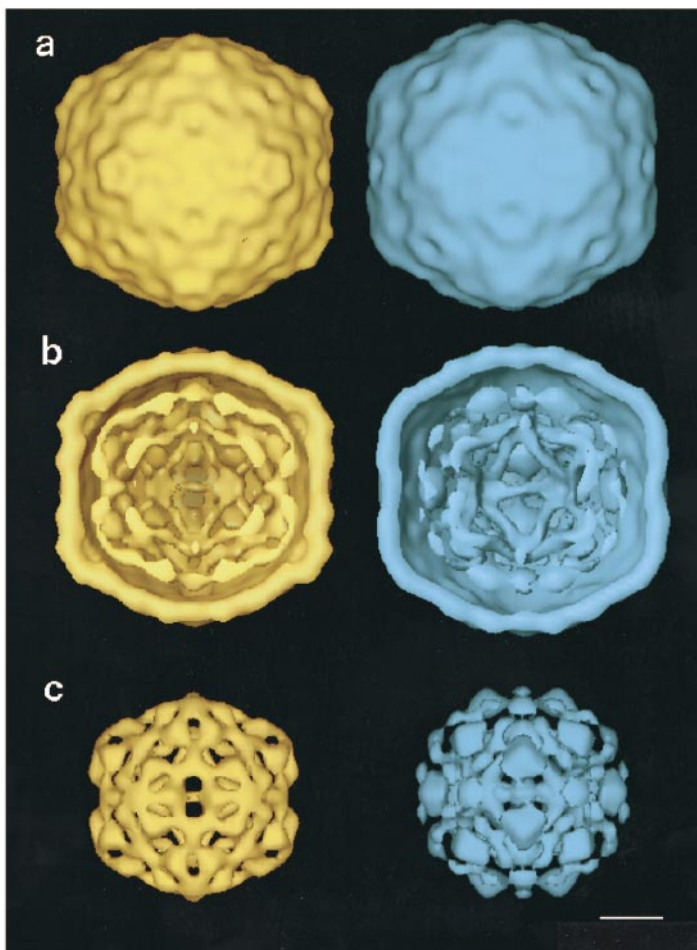


Figure 11. (a) Three-dimensional surface-shaded density maps of native (left, yellow) and expanded RYMV (right, blue) viewed down a 2-fold symmetry axis. The expanded particle has similar surface topography but is rounder than the native particle. (b) Sectioned views of both the native and expanded particles show internal density that we attribute to ordered genomic RNA, which has been displayed separately in (c). Note that particle expansion is associated with loss of the cavity beneath the 5-fold symmetry axes. The scale bar represents 40 Å.

single micrograph were determined using cross-correlation and common line procedures (Crowther, 1971; Fuller, 1987; Baker *et al.*, 1988; Olson & Baker, 1989). To optimize the search procedure, calculations were performed using only a portion of the Fourier transform of the masked image (between $1/70$ and $1/35 \text{ \AA}^{-1}$) to remove both low and high frequency noise. Three particles with well-defined orientations ($\sim 20^\circ$ phase residual) were used to compute an initial three-dimensional reconstruction using Fourier-Bessel inversion (Crowther, 1971). This initial map at 35 \AA resolution was used as the starting model for the Polar Fourier Transform (PFT) method (Baker & Cheng, 1996). Briefly, the Fourier transform of the density distribution of the particles was computed at each radius. A restricted range of particle radii (111 to 160 \AA) corresponding to radii encompassing the capsid shell was selected to optimize the search procedure. In addition, images were low-pass and high-pass filtered to optimize the determination of the origin and orientation parameters (between $1/70$ and $1/35 \text{ \AA}^{-1}$). The success of each cycle of refinement was assessed using the program CMP05 (kindly provided by Drs Tim Baker and Holland Cheng), which computes correlation coefficients comparing the density distribution of each particle with the corresponding projected view of the three-dimensional model. For the PFT method, 12 cycles (six in global mode with 1° increments and six in refinement mode with 0.5 and then 0.25° increments) were performed by progressively including more particles in the map and by extending the resolution in the refinement mode from 35 to 30 \AA . A

final map at 30 \AA resolution based on 12 particles was then used as a starting model to analyze a second micrograph of RYMV particle images. A similar PFT strategy yielded a three-dimensional map at 25 \AA resolution based on 50 particles.

For processing images of SCPMV particles, initial origin and orientation values were determined for 200 particles by cross-correlation and common lines procedures. A reconstruction at 35 \AA resolution based on five particles was used as a starting model for the PFT method. The calculations were performed by including radii of particle images between 120 and 170 \AA and by using the range of resolution as described above. Multiple cycles of refinement yielded a final three-dimensional map at 25 \AA resolution derived from 41 particles.

For processing the images of the expanded RYMV particles, the three-dimensional map of RYMV in the compact form was radially scaled to fit the radius of the expanded particles. This expanded map was used as the starting model for the PFT method. Multiple cycles of refinement, as described above, yielded a three-dimensional map at 35 \AA resolution derived from 23 particles. A similar strategy was attempted for processing the images of the expanded SCPMV particles. However, instability in the origin and orientation of particles during the search mode precluded determination of a reliable three-dimensional reconstruction.

To assess the resolution of the maps, each data set was divided in half to compute two independent reconstructions. The program EMMAP3DT was used to gener-

ate a list of structure factors, and the program EMCTF03 used these data to compute the correlation coefficient as a function of spatial frequency. All surface-shaded representations were visualized using AVS software (Sheehan *et al.*, 1996).

Fit between X-ray SCPMV model and cryo-EM maps

The program XPLOR (Brünger, 1996) was used to generate structure factors of the SCPMV X-ray model, and a map at 25 Å resolution was generated by inverse Fourier transformation using a temperature factor of 1000 Å². The program CMP05 was then used to determine a radial scale factor to fit the cryo-EM and X-ray map. The SCPMV cryo-EM map was contracted by 3%, and the RYMV cryo-EM map was expanded by 4.3% to best match the SCPMV X-ray map. Prior to performing the rigid-body refinement in XPLOR, the cryo-EM map was modified so that the density in the interior and exterior of the shell (presumably noise) was flattened to zero. The structure factors calculated from this modified density were used in XPLOR during refinement. Comparison of the structure factors for the unrefined X-ray model and the cryo-EM map of SCPMV yielded an *R*-factor of 0.56. After 40 cycles of rigid-body refinement wherein the three subunits, A, B, C of SCPMV, were allowed to move independently, the *R*-factor decreased to 0.36 for SCPMV and 0.28 for RYMV. The X-ray and cryo-EM maps were visualized using the program "O" (Jones *et al.*, 1991) to determine the view and select the non-crystallographic symmetry matrices (from the set of 60 icosahedral matrices) to generate selected Figures. The program Bobscript (Esnouf, 1997) was used for final rendering of the X-ray and cryo-EM maps in Figures 9 and 10.

Note added in proof

Since submission of this paper, the X-ray crystal structure of RYMV has been determined (C. Qu *et al.*, unpublished results). In spite of low sequence similarity with SCPMV, the coat protein of RYMV does fold as a canonical jellyroll β sandwich. However, a unique feature of RYMV explains the increased stability compared with SCPMV. The βA arms (residues 31-53) between 2-fold related C subunits are swapped with each other, thereby producing long-range interactions through the icosahedral surface lattice.

Acknowledgments

We thank S. Leitner for maintaining the plants. We thank Timothy S. Baker, Holland Cheng, James Conway, Tony Crowther and Alasdair Steven for computer programs. This work was supported by ORSTOM (French Scientific Research Institute for Development through Cooperation), by the Rockefeller Foundation, the National Institute of Health (AI27161 to R.N.B. and AI31535 to M.Y.), the Scripps Family Chair (to R.N.B.), the Gustavus and Louise Pfeiffer Research Foundation (to M.Y.) and the Donald E. and Delia B. Baxter Foundation (to M.Y.). During this work M.Y. was an Established Investigator of the American Heart Association and Bristol-Myers Squibb and is now the recipient of a Clinical Scholar Award in Translational Research from the Burroughs Wellcome Fund.

References

- Abad-Zapatero, C., Abdel-Meguid, S. S., Johnson, J. E., Leslie, A. G. W., Rayment, I., Rossmann, M. G., Suck, D. & Tsukihara, T. (1980). Structure of southern bean mosaic virus at 2.8 Å resolution. *Nature*, **286**, 33-39.
- Albert, F. G., Fox, J. M. & Young, M. J. (1997). Virion swelling is not required for cotranslational disassembly of cowpea chlorotic mottle virus *in vitro*. *J. Virol.* **71**, 4296-4299.
- Baker, T. S. & Cheng, R. H. (1996). A model-based approach for determining orientations of biological macromolecules imaged by cryoelectron microscopy. *J. Struct. Biol.* **116**, 120-130.
- Baker, T. S., Drak, J. & Bina, M. (1988). Reconstruction of the three-dimensional structure of simian virus 40 and visualization of the chromatin core. *Proc. Natl Acad. Sci. USA*, **85**, 422-426.
- Bakker, W. (1974). Characterization and ecological aspects of rice yellow mottle virus in Kenya. In *Agric. Res. Rep.* 829, p. 152, Cent. Agric. Publ. Doc, Wageningen.
- Bhuvaneshwari, M., Subramanya, H. S., Gopinath, K., Savithri, H. S., Nayudu, M. V. & Murthy, M. R. N. (1995). Structure of *Sesbania* mosaic virus at 3 Å resolution. *Structure*, **3**, 1021-1030.
- Bonneau, C., Brugidou, C., Chen, L., Beachy, R. N. & Fauquet, C. (1998). Expression of the rice yellow mottle virus P1 protein *in vitro* and *in vivo* and its involvement in virus spread. *Virology*, **244**, 79-86.
- Böttcher, B. & Crowther, R. A. (1996). Difference imaging reveals ordered regions of RNA in turnip yellow mosaic virus. *Structure*, **4**, 387-394.
- Brünger, A. T. (1996). Recent developments for crystallographic refinement of macromolecules. *Methods Mol. Biol.* **56**, 245-66.
- Canady, M. A., Larson, S. B., Day, J. & McPherson, A. (1996). Crystal structure of turnip yellow mosaic virus. *Nature Struct. Biol.* **3**, 771-781.
- Chauvin, C., Witz, J. & Jacrot, B. (1978). The structure of tomato bushy stunt virus: a model for protein-RNA interaction. *J. Mol. Biol.* **124**, 641-651.
- Chen, Z., Stauffacher, C., Li, Y., Schmidt, T., Bomu, W., Kamer, G., Shanks, M., Lomonosoff, G. & Johnson, J. E. (1989). Protein-RNA interactions in an icosahedral virus at 3.0 Å resolution. *Science*, **245**, 154-159.
- Crowther, R. A. (1971). Procedures for three-dimensional reconstruction of spherical viruses by Fourier synthesis from electron micrographs. *Phil. Trans. Roy. Soc. ser. B*, **261**, 221-230.
- Crowther, R. A., DeRosier, D. J. & Klug, A. (1970). The reconstruction of a three-dimensional structure from projections and its applications to electron microscopy. *Proc. Roy. Soc. ser. A*, **317**, 319-340.
- Esnouf, R. M. (1997). An extensively modified version of MolScript that includes greatly enhanced coloring capabilities. *J. Mol. Graph. Model.*, **15**, 132-134, (112-113 color plates).
- Fauquet, C. & Thouvenel, J. C. (1977). Identification of rice yellow mottle virus in Ivory Coast. *Plant Dis. Rep.* **61**, 443-446.
- Francki, R. I. B., Milne, R. G. & Hatta, T. (1985). *Atlas of Plant Viruses*, vol. 1, CRC Press, Boca Raton, FL, USA.
- Fricks, C. E. & Hogle, J. M. (1990). Cell-induced conformational change in poliovirus: externalisation of the amino terminus of VP1 is responsible for liposome binding. *J. Virol.* **64**, 1934-1945.

- Fuller, S. D. (1987). The $T = 4$ envelope of Sindbis virus is organized by interactions with a complementary $T = 3$ capsid. *Cell*, **48**, 923-934.
- Hogle, J. M., Maeda, A. & Harrison, S. C. (1986). Structure and assembly of turnip crinkle virus. I. X-ray crystallographic structure analysis at 3.2 Å resolution. *J. Mol. Biol.* **191**, 625-638.
- Hsu, C. H., Sehgal, O. P. & Pickett, E. E. (1976). Stabilizing effect of divalent metal ions on virions of southern bean mosaic virus. *Virology*, **69**, 587-595.
- Hull, R. (1977). The stabilization of the particles of turnip rosette virus and of other members of the southern bean mosaic virus group. *Virology*, **79**, 58-66.
- Jeffries, A. C., Rathjen, J. P. & Symons, R. H. (1995). Lucerne transient streak virus: complete genome, NCBI # U31286.
- Johnson, J. E., Rossmann, M. G., Smiley, I. E. & Wagner, M. A. (1974). Single crystal X-ray diffraction studies of southern bean mosaic virus. *J. Ultrastruct. Res.* **46**, 441-451.
- Jones, T. A., Zou, J.-Y., Cowan, S. W. & Kjeldgaard, M. (1991). Improved methods for building protein models in electron density maps and the location of errors in these models. *Acta Crystallog. sect. A*, **47**, 110-119.
- Krüse, J., Timmins, P. A. & Witz, J. (1982). A neutron scattering study of the structure of compact and swollen forms of southern bean mosaic virus. *Virology*, **119**, 42-50.
- Mäkinen, K., Tamm, T., Næss, V., Truve, E., Puurand, Ü., Munthe, T. & Saarma, M. (1995). Characterization of cocksfoot mottle sobemovirus genomic RNA and sequence comparison with related virus. *J. Gen. Virol.* **76**, 2817-2825.
- Ngon a Yassi, M., Ritzenthaler, C., Brugidou, C., Fauquet, C. & Beachy, R. N. (1994). Nucleotide sequence and genome characterization of rice yellow mottle virus RNA. *J. Gen. Virol.* **75**, 249-257.
- Olson, A. J., Bricogne, G. & Harrison, S. C. (1983). Structure of tomato bushy stunt virus IV. The virus particle at 2.9 Å resolution. *J. Mol. Biol.* **171**, 61-93.
- Olson, N. H. & Baker, T. S. (1989). Magnification calibration and the determination of spherical virus diameters using cryo-electron microscopy. *Ultramicroscopy*, **30**, 281-298.
- Olson, N. H., Baker, T. S., Johnson, J. E. & Hendry, D. A. (1990). The three-dimensional structure of frozen-hydrated *Nudaurelia capensis* β virus, a $T = 4$ insect virus. *J. Struct. Biol.* **105**, 111-122.
- Opalka, N., Brugidou, C., Bonneau, C., Nicole, M., Beachy, R. N., Yeager, M. & Fauquet, C. (1998). Movement of rice yellow mottle virus between xylem cells through pit membranes. *Proc. Natl Acad. Sci. USA*, **95**, 3323-3328.
- Othman, Y. & Hull, R. (1995). Nucleotide sequence of the bean strain of southern bean mosaic virus. *Virology*, **206**, 287-297.
- Prasad, B. V. V., Rothnagel, R., Zeng, C. Q.-Y., Jakana, J., Lawton, J. A., Chiu, W. & Estes, M. K. (1996). Visualization of ordered genomic RNA and localization of transcriptional complexes in rotavirus. *Nature*, **382**, 471-473.
- Rayment, I., Johnson, J. E. & Rossmann, M. G. (1979). Metal-free southern bean mosaic virus crystals. *J. Biol. Chem.* **254**, 5243-5245.
- Robinson, I. K. & Harrison, S. C. (1982). Structure of the expanded state of tomato bushy stunt virus. *Nature*, **297**, 563-568.
- Savithri, H. S. & Erickson, J. W. (1983). The self-assembly of the cowpea strain of southern bean mosaic virus: formation of $T = 1$ and $T = 3$ nucleoprotein particles. *Virology*, **126**, 328-335.
- Sheehan, B., Fuller, S. D., Pique, M. E. & Yeager, M. (1996). AVS software for visualization in molecular microscopy. *J. Struct. Biol.* **116**, 99-106.
- Shepherd, R. J. & Fulton, R. W. (1962). Identity of a seed-borne virus of cowpea. *Phytopathology*, **52**, 489.
- Silva, A. M. & Rossmann, M. G. (1987). Refined structure of southern bean mosaic virus at 2.9 Å resolution. *J. Mol. Biol.* **197**, 69-87.
- Speir, J. A., Munshi, S., Wang, G., Baker, T. S. & Johnson, J. E. (1995). Structures of the native and swollen forms of cowpea chlorotic mottle virus determined by X-ray crystallography and cryo-electron microscopy. *Structure*, **3**, 63-78.
- Wilson, T. M. A. (1985). Nucleocapsid disassembly and early gene expression by positive-strand RNA viruses. *J. Gen. Virol.* **66**, 1201-1207.
- Wu, S., Rinehart, C. A. & Kaesberg, P. (1987). Sequence and organization of southern bean mosaic virus genomic RNA. *Virology*, **161**, 73-80.
- Yeager, M., Dryden, K. A., Olson, N. H., Greenberg, H. B. & Baker, T. S. (1990). Three-dimensional structure of rhesus rotavirus by cryoelectron microscopy and image reconstruction. *J. Cell Biol.* **110**, 2133-2144.
- Yeager, M., Berriman, J. A., Baker, T. S. & Bellamy, A. R. (1994). Three-dimensional structure of the rotavirus haemagglutinin VP4 by cryo-electron microscopy and difference map analysis. *EMBO J.* **13**, 1011-1018.

Edited by W. Baumeister

(Received 18 May 2000; accepted 6 June 2000)